crystals

MDPI

*Article*

# Optical Spectroscopy of $Li_6Y(BO_3)_3$ Single Crystals Doped with Dysprosium

**Éva Tichy-Rács [1], Ivo Romet [2], László Kovács [1,*], Krisztián Lengyel [1], Gábor Corradi [1] and Vitali Nagirnyi [2]**

[1] Wigner Research Centre for Physics, Konkoly-Thege út 29-33, H-1121 Budapest, Hungary; tichy-racs.eva@wigner.hu (É.T.-R.); lengyel.krisztian@wigner.hu (K.L.); corradi.gabor@wigner.hu (G.C.)
[2] Institute of Physics, University of Tartu, W. Ostwald Str. 1, 50411 Tartu, Estonia; ivoromet@gmail.com (I.R.); vitali.nagirnoi@ut.ee (V.N.)
* Correspondence: kovacs.laszlo@wigner.hu; Tel.: +36-1-392-2588

**Abstract:** The energy levels of $Dy^{3+}$ ions have been determined in lithium yttrium borate ($Li_6Y(BO_3)_3$) single crystals in a wide spectral range between 3000 and 40,000 $cm^{-1}$ using optical absorption and luminescence spectroscopy, which also allow for an analysis of the ground state. The crystal field splittings of the $^6H_{15/2}$ ground state and all excited states up to the $^4F_{7/2}$ manifold were obtained at a low temperature, based on luminescence (T = 4.2–78 K) and absorption (T = 8–100 K) measurements, respectively. The numbers of experimentally observed Stark sublevels are in agreement with those expected theoretically for $Dy^{3+}$ ions occupying a single low symmetry ($C_1$) site.

**Keywords:** FTIR absorption spectra; luminescence spectra; single crystals; dysprosium; lithium yttrium borate



**Citation:** Tichy-Rács, É.; Romet, I.; Kovács, L.; Lengyel, K.; Corradi, G.; Nagirnyi, V. Optical Spectroscopy of $Li_6Y(BO_3)_3$ Single Crystals Doped with Dysprosium. *Crystals* **2021**, *11*, 503. https://doi.org/10.3390/cryst11050503

Academic Editor: Shin-ichi Kimura

Received: 27 March 2021
Accepted: 26 April 2021
Published: 2 May 2021



## 1. Introduction

Borate crystals often demonstrate advantageous properties such as high optical quality, transparency in a wide spectral range including vacuum ultraviolet (VUV), and optical nonlinearity. For this reason, they are recognized as good matrices for laser applications [1–3]. Some of these, e.g., lithium borates, are attractive materials for neutron detectors due to the presence of naturally abundant $^6Li$ and $^{10}B$ isotopes [4–9]. Lithium yttrium borate ($Li_6Y(BO_3)_3$, LYB) has been suggested as a phosphor, laser, or scintillator material depending on the host morphology and rare-earth (RE) ion doping [10–13]. This compound with monoclinic crystal structure of the $P2_1/c$ space group (Z = 4) [14] and the unit cell parameters a = 7.157(5) Å, b = 16.378(4) Å, c = 6.623(4) Å, β = 105.32(5)° [15] is an excellent host for RE doping, since it contains yttrium sites of only one type which can incorporate any RE dopant without concentration restrictions, as all $Li_6RE(BO_3)_3$ crystals are isostructural with $Li_6Y(BO_3)_3$ [16]. The $Y^{3+}$ sites form a zigzag chain along the crystallographic <001> direction with a distance of 3.85 Å between the closest neighbors and ~7 Å between the chains. This anisotropy of the $Li_6RE(BO_3)_3$ crystal structure causes a dominant one-dimensional energy transfer and prevents concentration quenching of RE luminescence [17]. In $Li_6Y(BO_3)_3$:Yb crystals, the absence of emission quenching has been proven for concentrations up to 20 mol% of Yb, whereas unlike powders, crystals demonstrate a remarkable lengthening of the decay time of the RE emission with concentration, which is related to the reabsorption and repeated emission process taking place within the impurity complex [18]. The trivalent $Dy^{3+}$ is a promising RE dopant because of its relatively strong white-light emission which is important for laser, display panel, and telecommunication applications [19–21]. Some of the RE ions have already been extensively studied in various host crystals in view of their potential application as a medium for coherent quantum dynamics (e.g., praseodymium in yttrium silicate in resonant nonlinear optical experiments [22]). $Dy^{3+}$ is a perspective candidate in this field, since it has shown highly efficient APTE (Addition de Photons par Transferts d'Energie) up-conversion luminescence

in $Yb^{3+}$ doped compounds containing $Dy^{3+}$ ions even at trace levels [18,23]. This sensitive energy transfer to the $Dy^{3+}$ ions through the excited $Yb^{3+}$ states and a stable borate host matrix establish the potential of using dysprosium doped LYB crystals in quantum optical experiments. Preliminary spectroscopic studies of Dy-doped $Li_6Y(BO_3)_3$ have been performed for polycrystalline phosphors [10], glasses [12], and recently, single crystals [24]. These studies revealed the spectral positions and temporal characteristics of the main electronic transitions of $Dy^{3+}$ in the material, however, did not provide information on fine structure of the transitions necessary to fully identify the crystal field splitting of $Dy^{3+}$ ion states introduced in such an anisotropic matrix. In the present work, the results of high-resolution absorption and luminescence measurements aimed at identifying the Stark levels of $Dy^{3+}$ ions in LYB crystals are presented.

## 2. Experimental

$Li_6Y(BO_3)_3$ single crystals doped with 1 and 5 mol% dysprosium were grown by the Czochralski method detailed in [25] (Figure 1). To synthesize the starting charge, $Li_2CO_3$ (99.9%), $Y_2O_3$ (99.9%), $B_2O_3$ (Merck pro analysis) and $Dy_2O_3$ (99.9%) powders were mixed in the ratio of constituents expected for bulk crystal and placed into a silver crucible. The mixtures were annealed at 580 °C for 42 h and at 650 °C for 12 h. Between the reaction steps applied, the samples were weighed and reground. The synthesized material was finely ground and placed into a gold-coated platinum crucible. Crystals were grown from this crucible in air, using a resistance-heated furnace fitted with a diameter-controlled growth apparatus. The crystals were pulled along the b = <010> axis, with a rate of 0.16 mm/h and a rotation speed of 8–14 rpm. Samples oriented by X-ray diffraction were prepared in the form of thin slices with a thickness of about 1–2 mm with their large faces perpendicular or parallel to the growth direction. In the latter case, the plane of the slice coincides with the $(\bar{1}02)$ Miller plane which is nearly perpendicular to the dielectric z-axis, according to [26].

(**a**) (**b**)

**Figure 1.** 1 mol% (**a**) and 5 mol% (**b**) Dy doped $Li_6Y(BO_3)_3$ single crystals grown by the Czochralski method. The cylindrical part is 30 mm long and 25 mm in diameter.

The absorption spectra were recorded by BRUKER IFS 66v and 120 FTIR Fourier transform spectrophotometers (Bruker, Ettlingen, Germany) with resolution of 0.2 $cm^{-1}$ and 0.05 $cm^{-1}$, respectively. A closed cycle He cryostat equipped with KRS-5 and quartz windows (Specac, Orpington, England) for measurements in different wavenumber regions was used to perform the low temperature (≈8 K) studies. KRS-5 and quartz polarizers (Specac, Orpington, England) were utilized to investigate the anisotropy of the $Dy^{3+}$ electronic transitions in the monoclinic LYB lattice.

The steady-state and time-resolved photoluminescence studies were carried out at the Institute of Physics, University of Tartu, using a custom-made setup using a 400 W deuterium discharge lamp DDS-400 (Vladikavkaz electric lamp plant, Vladikavkaz, Russia) or a Xe flash-lamp PerkinElmer 150 W (Perkin Elmer Optoelectronics, Wiesbaden, Germany) for sample excitation, respectively. The excitation wavelength was selected with a double-quartz prism-monochromator DMR-4 (Kazan Optical-Mechanical Plant, Kazan, Russia). The samples were mounted in a Janis VPF-800 liquid nitrogen cryostat (78–800 K) (Janis

Research Company, Woburn, England) or in a liquid helium cryostat (1.8–400 K) (Low Temperature Laboratory, Tartu, Estonia) by means of a specially designed spring-equipped copper finger or with conductive silver glue, respectively. Luminescence spectra were studied using an ARC Spectra Pro 308i (Acton Research Corporation, Acton, England) Czerny-Turner type grating monochromator equipped with a Princeton Instruments CCD camera (Teledyne Princeton Instruments, Krailing, Germany) or a Hamamatsu H6240-02 (Hamamatsu Photonics Norden AB, Solna, Sweden) photon counting head for the steady-state and time-resolved measurements, respectively. The spectral resolution was kept 1.08 nm for review luminescence spectra and 0.27 nm for detailed spectra. The luminescence detection technique is described in more detail in [27]. Photostimulated luminescence emission and excitation spectra were measured in the temperature interval 4.2–300 K, which was controlled by a LakeShore 335 device (Lake Shore Cryotonics, Inc., Westerville, OH, USA). Various SCHOTT (Edmund Optics, Mainz, Germany) or UQG Optics (UQG Optics, Cambridge, England) colour glass filters were used to additionally suppress possible effects of stray light or second orders of excitation and emission light. The excitation spectra were normalized to the reference signal of sodium salicylate to equalize the quantum intensities of incident light at different photon energies. The emission spectra were corrected for the monochromator spectral efficiency and spectral sensitivity of the detector.

## 3. Results and Discussion

### *3.1. Absorption Spectra*

To characterize the incorporation of dysprosium impurity into the host, the absorbances of LYB crystals doped with $Dy^{3+}$ ions in concentrations of 1 and 5 mol% were compared using samples of identical thickness and orientation. The absorption bands in the 7000–10,000 $cm^{-1}$ wavenumber range corresponding to the electronic transitions from the $^6H_{15/2}$ ground state to the $^6H_{9/2}$, $^6F_{11/2}$, $^6H_{7/2}$, and $^6F_{9/2}$ terms of the excited state can be seen in Figure 2. The amplitude of the absorption bands measured in the LYB:Dy(5 mol%) crystal was by a factor of five higher than that in LYB:Dy(1 mol%). This confirms that the distribution coefficient of $Dy^{3+}$ ions is the same in both cases and does not depend on the Dy concentration in the melt (see also [15]).

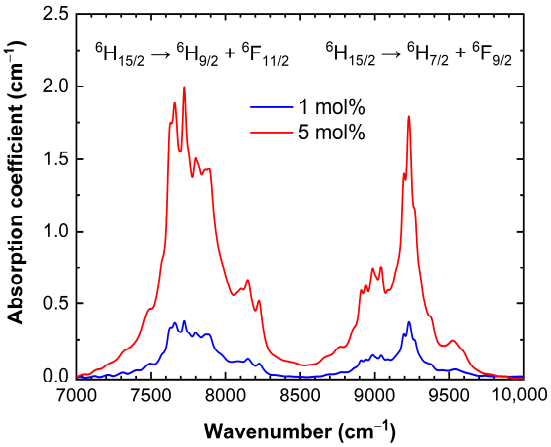


**Figure 2.** The absorbance of 1 and 5 mol% $Dy^{3+}$ doped LYB crystals in the 7000–10,000 $cm^{-1}$ spectral range measured at room temperature. The absorption coefficient of the 5 mol% $Dy^{3+}$ doped crystal is about five times higher compared to that of the 1 mol% doped LYB.

To determine the fine structure of $Dy^{3+}$ electronic transitions, detailed high-resolution measurements were performed at a low temperature. The absorption spectra of LYB:Dy (5 mol%) crystal in the 3000–40,000 $cm^{-1}$ wavenumber range present a sequence of narrow bands with a minimum halfwidth of about 1 $cm^{-1}$ at T = 8 K. The absorption bands correspond to the transitions from the lowest sublevel of the $^6H_{15/2}$ ground state to the excited energy levels of the $Dy^{3+}$ ions, which can be easily assigned using the Dieke

diagram [28] up to the $^4F_{7/2}$ multiplet at about 25,000 cm$^{-1}$. Because of the monoclinic crystal structure of LYB, all energy levels of $Dy^{3+}$ split into the maximum possible number of Stark components separated by about 100–600 cm$^{-1}$. As a consequence, the Stark components of various nearby levels are mixed and cannot be unambiguously assigned, especially at high energies above 29,000 cm$^{-1}$ (see, e.g., Figure 3g,h). Some doubtful assignments based on the excitation spectrum of a LYB:Dy crystal can be found in the paper by Saha et al. [24]. Difficulties in the determination of the proper energy terms have also been encountered for other monoclinic crystals, such as $KY(WO_4)_2$ and $Lu_2SiO_5$, doped with $Dy^{3+}$ ions [29,30]. Most of the spectral lines experimentally observed in LYB:Dy in the present work are shown in Figure 3 and the most probable assignments are listed in Table 1. Beside the electronic transitions of $Dy^{3+}$ ions some additional weak absorption bands attributed to the stretching vibration of hydroxyl ion ($OH^-$) impurities can be observed between 3450–3560 cm$^{-1}$ as shown in Figure 3a. According to our measurements, these bands are present in undoped and other RE ion doped LYB crystals as well. The uneven baseline in this wavenumber range is related to the absorption of higher harmonics of the B-O vibrations in the host crystal.

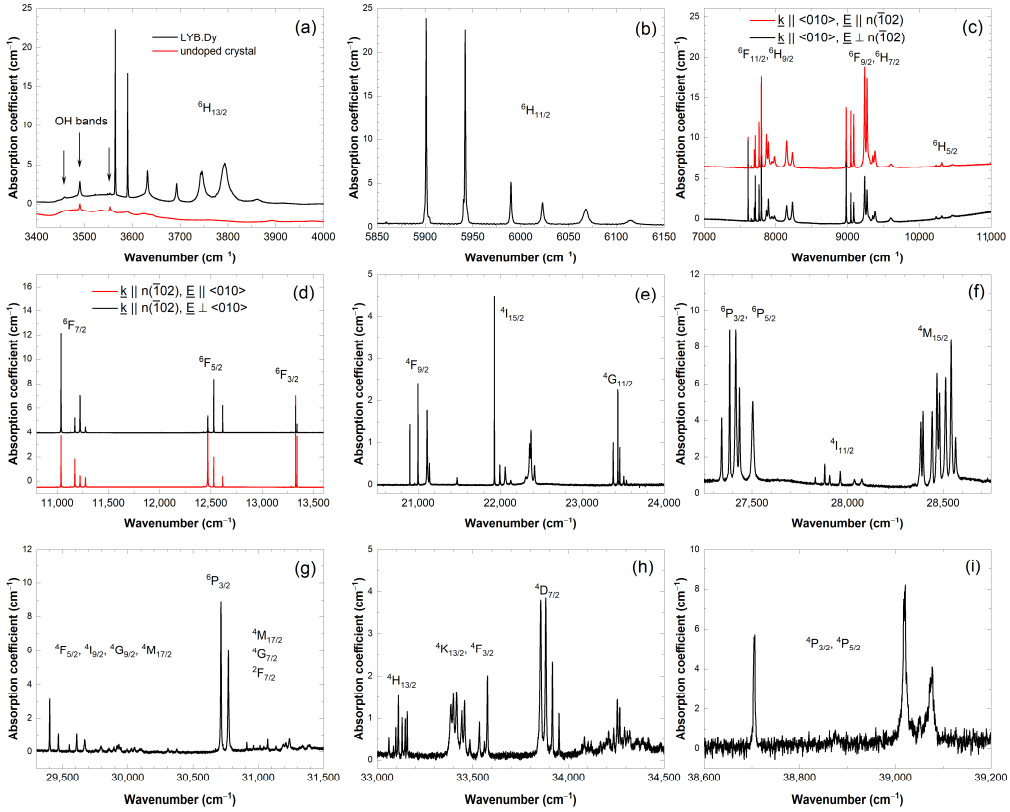


**Figure 3.** Absorption spectra of $Dy^{3+}$ ions in LYB:Dy(5 mol%) single crystal measured in the infrared (**a**–**d**), visible (**e**) and UV (**f**–**i**) spectral range at T = 8 K. Transitions from the lowest level of the $^6H_{15/2}$ ground state to various multiplets are indicated.

Figure 3a–c,e–i shows the high-resolution absorption spectra of LYB:Dy(5 mol%) crystal recorded for light propagating along the <010> axis of the crystal. The spectra for light propagating along the n$(\bar{1}02)$ direction with polarization parallel and perpendicular to the <010> direction are shown in Figure 3d. All lines related to the fully split Stark components are clearly visible for both polarizations, only their relative intensities vary slightly. The number of experimental bands is in full agreement with theoretical predictions; the exact positions of the lines obtained from experiment are given in Table 1. Since no additional absorption lines appear in the low-temperature spectra, only one type of site can be assumed for $Dy^{3+}$ ions in the LYB lattice, as expected due to the isostructural property

of $Li_6RE(BO_3)_3$ crystals [16]. The same conclusion was drawn also from the optical and electron paramagnetic resonance (EPR) spectroscopy of $Er^{3+}$ doped LYB crystals [31].

**Table 1.** Energy levels of $Dy^{3+}$ ions in monoclinic $Li_6Y(BO_3)_3$ crystals (in $cm^{-1}$).

| | 1 | 2 | 3 | 4 | 5 | 6 | 7 | 8 | 9 | 10 | $N_{theory}$ | ΔE |
|---|---|---|---|---|---|---|---|---|---|---|---|---|
| $^6H_{15/2}$ | 0 | 42 | 79 | 134 | 244 | 389 | 503 | 598 | | | 8 | 598 |
| $^6H_{13/2}$ | 3564.7 | 3590.5 | 3631.8 | 3692.9 | 3745.8 | 3794.0 | 3861.7 | | | | 7 | 297 |
| $^6H_{11/2}$ | 5901.2 | 5941.9 | 5989.8 | 6022.8 | 6068.0 | 6115.0 | | | | | 6 | 214 |
| $^6H_{9/2} + {}^6F_{11/2}$ | 7613.4 | 7698.9 | 7713.5 | 7766.0 | 7798.5 | 7870.0 | 7896.5 | 7947.2 | 7980.9 | 8151.1 | 11 | 619 |
| | 8232.1 | | | | | | | | | | | |
| $^6H_{7/2} + {}^6F_{9/2}$ | 8980.3 | 9045.2 | 9085.5 | 9237.6 | 9270.9 | 9299.0 | 9350.0 | 9382.0 | 9602.0 | | 9 | 622 |
| $^6H_{5/2}$ | 10,233.0 | 10,312.0 | 10,460.0 | | | | | | | | 3 | 223 |
| $^6F_{7/2}$ | 11,038.6 | 11,173.1 | 11,223.9 | 11,276.9 | | | | | | | 4 | 238 |
| $^6F_{5/2}$ | 12,470.0 | 12,528.4 | 12,615.5 | | | | | | | | 3 | 135 |
| $^6F_{3/2}$ | 13,327.2 | 13,340.7 | | | | | | | | | 2 | 13.5 |
| $^6F_{1/2}$ | 13,873.6 | | | | | | | | | | 1 | 0 |
| $^4F_{9/2}$ | 20,897 | 20,997 | 21,108 | 21,136 | 21,473 | | | | | | 5 | 576 |
| $^4I_{15/2}$ | 21,928.7 | 21,995 | 22,061 | 22,130 | 22,313 | 22,359 | 22,375 | 22,418 | | | 8 | 489 |
| $^4G_{11/2}$ | 23,378 | 23,434 | 23,458 | 23,507 | 23,539 | 23,596 | | | | | 6 | 218 |
| $^4F_{7/2}$ | 24,769 | 24,834 | 24,916 | 24,935 | | | | | | | 4 | 166 |
| $^4I_{13/2}$–$^4M_{19/2}$ | about 20 lines | | | | | | | | | | | |
| $^6P_{5/2} + {}^6P_{3/2}$ | 27,342 | 27,384 | 27,415 | 27,435 | 27,504 | | | | | | 5 | 162 |
| $^4I_{11/2}$ | 27,831 | 27,880 | 27,906 | 27,962 | 28,036 | 28,074 | | | | | 6 | 243 |
| $^4M_{15/2}$ | 28,382 | 28,394 | 28,442 | 28,467 | 28,480 | 28,512 | 28,541 | 28,565 | | | 8 | 183 |
| $^6P_{7/2}$–$^2F_{7/2}$ | about 40 lines | | | | | | | | | | | |
| $^4H_{13/2}$ | 33,061 | 33,084 | 33,097 | 33,110 | 33,130 | 33,146 | 33,156 | | | | 7 | 95 |
| $^4K_{13/2} + {}^4F_{3/2}$ | 33,384 | 33,398 | 33,415 | 33,442 | 33,456 | 33,484 | 33,533 | 33,560 | 33,576 | | 9 | 192 |
| $^4D_{7/2}$ | 33,854 | 33,881 | 33,916 | 33,950 | | | | | | | 4 | 96 |
| $^4F_{5/2}$–$^4F_{3/2}$ | about 25–30 lines | | | | | | | | | | | |
| $^4P_{5/2} + {}^4P_{3/2}$ | 38,705 | 38,875 | 39,019 | 39,050 | 39,074 | | | | | | 5 | 369 |

It is remarkable that upon gradually increasing the temperature from 8 to 100 K, additional lines appear in the absorption spectrum, which can be related to the transitions from thermally populated higher states of the $^6H_{15/2}$ ground state of $Dy^{3+}$ to various terms of the excited state. Figure 4 demonstrates this on the example of the $^6H_{15/2} \rightarrow {}^6F_{5/2}$ transition. At the lowest temperatures nearly exclusively the lines at 12,470, 12,528.4, and 12,605.5 $cm^{-1}$, corresponding to transitions from the lowermost Stark level of the $^6H_{15/2}$ ground state, are seen. As the higher sublevels of the ground state become populated at elevated temperatures, additional repetitions for these transitions appear at wavenumbers less by the same amounts (42, 79, and 134 $cm^{-1}$) corresponding to transitions from some of the higher Stark levels of the ground state to unchanged excited states. The positions of these hot replicas are helpful for identifying the lowest energy Stark levels of the ground state to be situated at 42, 79, and 134 $cm^{-1}$. The higher energy crystal field components of the ground state were determined from luminescence measurements (see below).

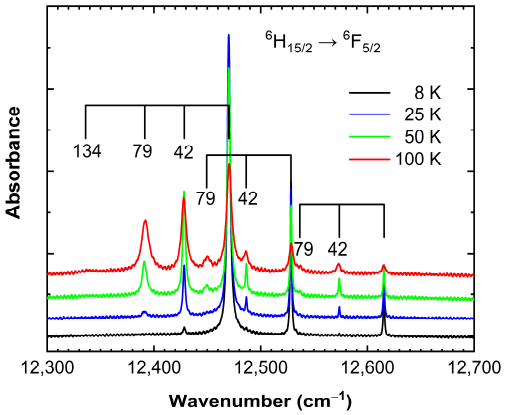


**Figure 4.** Temperature dependence of the $^6H_{15/2} \rightarrow {}^6F_{5/2}$ transition of $Dy^{3+}$ ions in the LYB:Dy(1 mol%) crystal. The hot bands show that the lowest energy crystal field components of the ground state are found at 42, 79 and 134 cm$^{-1}$.

### 3.2. Luminescence

Additional information on the position of high-energy excited $Dy^{3+}$ states was obtained from the studies of low-temperature luminescence and excitation spectra for the LYB:Dy(1 mol%) crystal. To record the luminescence spectra, the excitation wavelength was chosen at 356 nm (28,068 cm$^{-1}$), which populated the $^4I_{11/2}$ multiplet and provided the highest emission intensity. Upon the excitation of this term, electrons relax to the $^4F_{9/2}$ multiplet via nonradiative transitions, therefore, the transitions originating from the latter were further investigated in detail (see Figure 5b). The excitation spectrum was recorded for the most intense line at $\lambda_{em}$ = 577 nm (17,331 cm$^{-1}$) of the $^4F_{9/2} \rightarrow {}^6H_{13/2}$ transition. The emission and excitation spectra measured at temperatures 4.2 K or 78 K are presented in Figures 5–8, respectively. Figure 5a shows the overview of the emission spectrum in the region of 11,000–22,000 cm$^{-1}$. Two major bands centered at about 20,620 and 17,240 cm$^{-1}$ related to the $^4F_{9/2} \rightarrow {}^6H_{15/2}$ and $^4F_{9/2} \rightarrow {}^6H_{13/2}$ transitions, respectively, dominate the spectrum. Three weaker groups of bands observed approximately at 15,040, 13,160, and 11,770 cm$^{-1}$ in the near-infrared region are assigned to the $^4F_{9/2} \rightarrow {}^6H_{11/2}$, $^4F_{9/2} \rightarrow {}^6H_{9/2}$,$^6F_{11/2}$ and $^4F_{9/2} \rightarrow {}^6H_{7/2}$,$^6F_{9/2}$ transitions, respectively (Figure 5a,b). The positions of the main emission bands are in good agreement with those reported earlier for $Li_6Y(BO_3)_3$:Dy [10,12,24] and various other systems, such as phosphate glasses, molybdates and vanadates [32–34].

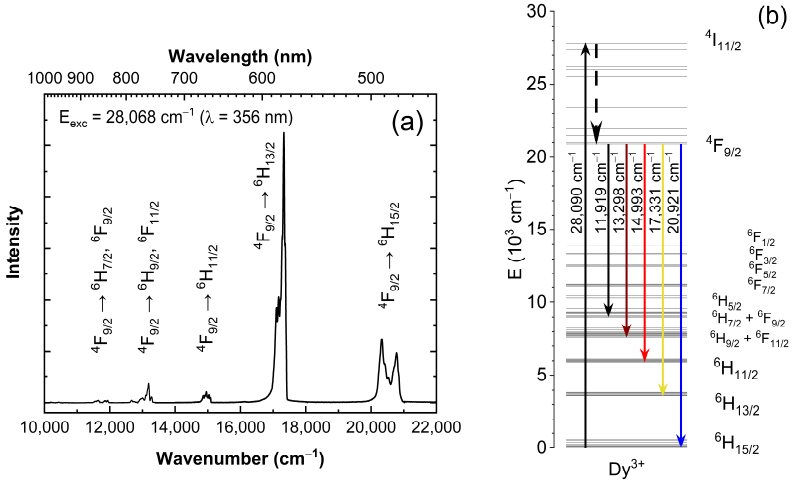


**Figure 5.** (**a**) Overview of the luminescence spectrum measured for $Li_6Y(BO_3)_3$:Dy(1 mol%) single crystal under excitation at 28,068 cm$^{-1}$ at 4.2 K. (**b**) Energy level diagram of $Dy^{3+}$ ions in LYB crystal showing the excitation from the ground state and various emission lines.

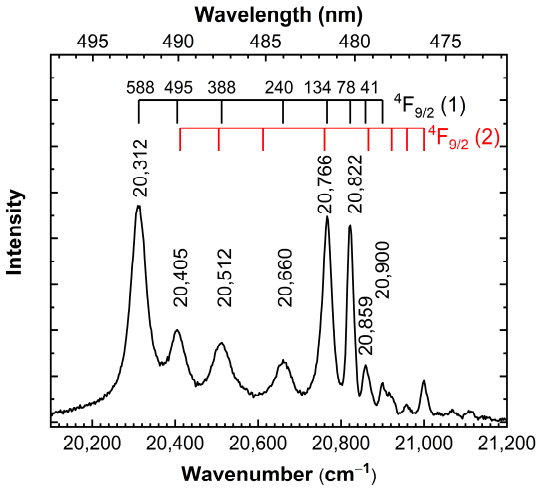


**Figure 6.** A detailed part of the luminescence spectrum at T = 78 K corresponding to the $^4F_{9/2} \rightarrow {}^6H_{15/2}$ transition. The numbered scale (1) on the top proves the correspondence of the luminescence transitions to the Stark components of the ground $^6H_{15/2}$ state partly found from absorption. Scale (2) corresponds to a hot state of the $^4F_{9/2}$ multiplet.

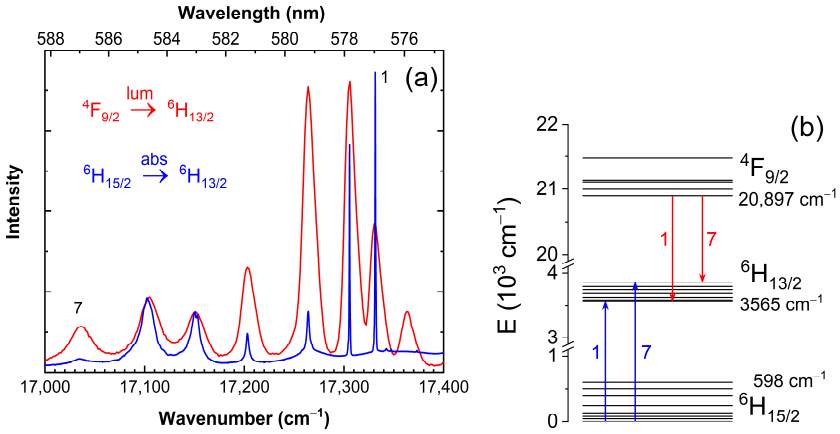


**Figure 7.** (**a**) The $^4F_{9/2} \rightarrow {}^6H_{13/2}$ luminescence transitions at T = 78 K (red line) and the absorption spectrum presented in Figure 3a but reversed as described in the text (blue line). (**b**) Part of the energy levels showing the absorption and luminescence transitions.

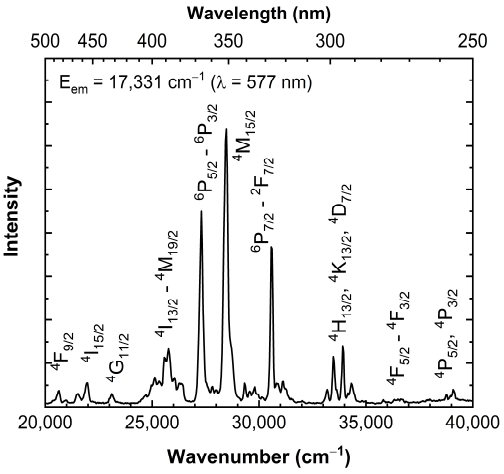


**Figure 8.** Excitation spectrum between 20,000–40,000 cm$^{-1}$ recorded at T = 78 K for the $^4F_{9/2} \rightarrow {}^6H_{13/2}$ emission at 17,331 cm$^{-1}$ in the LYB:Dy(1 mol%) single crystal.

The shape of the bands responsible for the $^4F_{9/2} \rightarrow {}^6H_{15/2}$ and $^4F_{9/2} \rightarrow {}^6H_{13/2}$ transitions varies in the above-cited works, and for that reason, zoomed spectrum parts measured with higher spectral resolution are shown for these transitions in more detail in Figures 6 and 7. The fine structure of these transitions is represented by 8 lines in the regions of 20,200–20,950 $cm^{-1}$ (Figure 6) and 7 lines in the region of 17,000–17,350 $cm^{-1}$ (Figure 7), respectively, in agreement with the number of crystal field components of the given multiplets $^6H_{15/2}$ and $^6H_{13/2}$. Weaker lines at higher wavenumber values in both Figures 6 and 7 are due to transitions from a hot state of the $^4F_{9/2}$ multiplet. The Stark components of the $^6H_{15/2}$ ground state can be determined from the $^4F_{9/2} \rightarrow {}^6H_{15/2}$ luminescence spectrum (see black scale (1) on top of Figure 6). The three lowest energy levels are in good agreement with those obtained from the hot bands in the absorption spectra measured at about T = 100 K (see, e.g., Figure 4). A few lines at wavenumber values higher than 20,900 $cm^{-1}$ may be related to the hot transitions originating from the second Stark component of the $^4F_{9/2}$ multiplet populated at 78 K (see red scale (2) on top of Figure 6).

The Stark components of the $^6H_{13/2}$ multiplet can be determined from both the absorption and luminescence measurements. It is remarkable, that the detailed structure of the $^4F_{9/2} \rightarrow {}^6H_{13/2}$ emission corresponds almost perfectly to the reversed absorption spectrum shown for the $^6H_{15/2} \rightarrow {}^6H_{13/2}$ transition at 8 K in Figure 3a. The reversion point was defined by the overlay of the emission line at 17,331 $cm^{-1}$ with the absorption line at 3564.7 $cm^{-1}$. This comparison demonstrates the consistency of the results obtained by the two spectroscopic methods.

The position of higher energy multiplets of the $Dy^{3+}$ ion in $Li_6Y(BO_3)_3$ may be obtained from the excitation spectra of the LYB:Dy(1 mol%) single crystal measured for the 17,331 $cm^{-1}$ emission line, one of the most intense ones in the series of the $^4F_{9/2} \rightarrow {}^6H_{13/2}$ transitions (Figure 8). The general features of the recorded excitation spectrum are in good agreement with the excitation spectra reported earlier for glass [12] and crystalline material [24], however, by using a better spectral resolution it was possible to ascribe the observed bands to specific levels of the higher-energy multiplets situated above 22,000 $cm^{-1}$.

According to [10,35,36] the $^4F_{9/2} \rightarrow {}^6H_{15/2}$ transition is an allowed magnetic dipole transition and the $^4F_{9/2} \rightarrow {}^6H_{13/2}$ transition belongs to a forced electric dipole transition being allowed only in the case when the $Dy^{3+}$ ion is located at a lattice site missing inversion center symmetry. Therefore, the fact that the group of yellow emission bands around 577 nm (17,331 $cm^{-1}$) is the most intense one in the spectrum confirms that $Dy^{3+}$ ions occupy $Y^{3+}$ sites in $Li_6Y(BO_3)_3$ single crystals, resulting in the hypersensitive ($^4F_{9/2} \rightarrow {}^6H_{13/2}$) transition. This is in accordance with the results reported earlier for the $Li_6Y(BO_3)_3$:$Dy^{3+}$ phosphor [10]. Indicatively, the ratio of the intensities of the $^4F_{9/2} \rightarrow {}^6H_{13/2}$ and $^4F_{9/2} \rightarrow {}^6H_{15/2}$ emissions is much lower in glass samples [12] than in crystals. This difference originates from the simple fact that single crystals possess an established structure characterized by a well-defined low-symmetry yttrium substitution site while the glass material allows a varying local crystal structure in the environment of $Y^{3+}$ ($Dy^{3+}$) ions. This conclusion is supported also by our studies of the decay kinetics of the emission at 17,331 $cm^{-1}$ under pulse excitation into the $^4M_{15/2}$ multiplet at 28,382 $cm^{-1}$ (Figure 9). We found two exponential components with decay times around 310 and 840 μs at 69 K. The integrated intensity of the faster component is very low, amounting only to 5% of the total emission intensity, so the emission decay is close to a single exponential which one can see also from Figure 9 presenting the decay curve in a semi-logarithmic scale. The decay time of the main component slightly increases to 910 μs at room temperature, while that of the shorter one increases approximately to 350 μs, whereas the ratio of their intensities remains the same. The nearly single exponential decay of the $Dy^{3+}$ emission confirms that the $Dy^{3+}$ ions occupy only one type of lattice sites as also expected in the $Li_6Y(BO_3)_3$ compound. A small admixture of a faster component is presumably related to a small fraction of $Dy^{3+}$ ions perturbed by a lattice defect, neighboring $Dy^{3+}$ ion or crystal surface. These results are similar to those obtained earlier for polycrystalline powder [10] and single crystal [24] samples, whereas in the latter, the increase of the average decay time with temperature

was also observed. In glass samples, on the contrary, a non-exponential decay with characteristics times depending on Dy concentration was observed reflecting non-equivalent positions of $Dy^{3+}$ ions and energy transfer between them in this material [12].

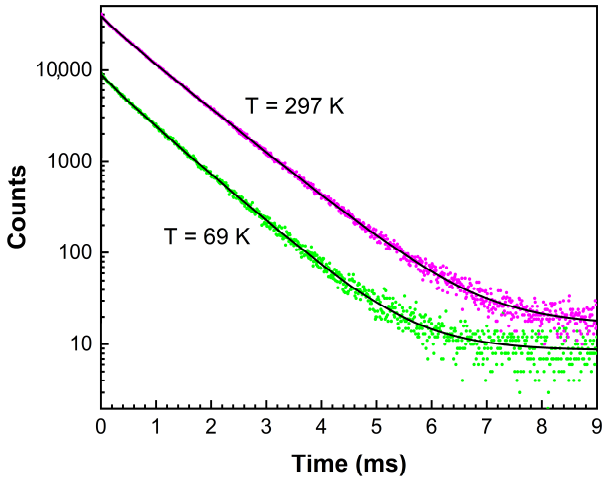


**Figure 9.** Decay curve of the emission at 17,331 $cm^{-1}$ under excitation at 28,382 $cm^{-1}$ at 69 and 297 K. Solid black curves present the results of curve fitting with two decay components listed in the text.

A full set of energy states determined from the absorption, emission, and excitation spectra in the present work is listed in Table 1. An energy diagram of the energy states observed is presented in Figures 5b and 7b accounting also for the splitting of the ground $^6H_{15/2}$ state. This splitting is well observed in the structure of the blue emission between 20,300–20,900 $cm^{-1}$ (Figure 5b) and in the temperature dependent absorption spectra (Figure 4).

The data shown in Table 1 present much more details on the splitting of excited state multiplets than reported in Refences [10,24]. The reason lies in the much higher resolution of our absorption measurements compared to that achieved in the measurements of excitation spectra in the cited papers. In addition to allowing for the determination of the Stark splitting of almost every multiplet, this was also helpful to better identify the multiplets themselves, especially in the energy regions where excited states are located at high densities (e.g., around 21,000, 28,000, and 37,000 $cm^{-1}$). Nevertheless, even the resolution achieved in our measurements was in some cases insufficient to resolve all lines in such energy regions. Therefore, in Table 1 we only present the estimated number of lines for the $^4I_{13/2}$–$^4M_{19/2}$, $^6P_{7/2}$–$^2F_{7/2}$, and $^4F_{5/2}$–$^4F_{3/2}$ terms. The relative positions of the multiplets detected in the present paper are in good agreement with those predicted for free $Dy^{3+}$ ions [28,37], and those determined for $Dy^{3+}$ ions in solutions [38,39].

## 4. Conclusions

Electronic transitions of $Dy^{3+}$ ions incorporated in the $Li_6Y(BO_3)_3$ crystals were successfully identified by absorption measurements in the wavenumber region of 3000–40,000 $cm^{-1}$ and luminescence excitation spectra measurements in the energy region of 18,500–40,000 $cm^{-1}$. The effect of crystal-field splitting in this low-symmetry crystal was investigated in detail by temperature and polarization dependent absorption and luminescence measurements. An intensive luminescence emission related to the $^4F_{9/2} \rightarrow {}^6H_{13/2}$ transitions was detected at 577 nm (17,331 $cm^{-1}$), testifying about the well-defined environments of $Dy^{3+}$ ions homogeneously substituted at $Y^{3+}$ sites lacking inversion symmetry. The splitting of the $^6H_{15/2}$ ground state of $Dy^{3+}$ was established and the energy diagram of the excited levels derived.

**Author Contributions:** Conceptualization, L.K.; methodology, L.K. and V.N.; investigation, É.T.-R., I.R., L.K., K.L. and V.N.; writing—original draft preparation, É.T.-R.; writing—review and editing, L.K., K.L., G.C. and V.N.; visualization, É.T.-R. and I.R.; funding acquisition, G.C. and V.N. All authors have read and agreed to the published version of the manuscript.

**Funding:** Part of this work was realized within the Quantum Information National Laboratory of Hungary supported by the Ministry of Innovation and Technology and the National Research, Development and Innovation Office (No. of Grant Agreement: NKFIH-873-3/2020). The financial support from the Cooperation Project of the Estonian and Hungarian Academies of Sciences, Estonian Research Council, project PUT PRG111, and the ERDF funding in Estonia granted to the Centre of Excellence TK141, Project No. 2014-2020.4.01.15-0011 is also acknowledged.

**Institutional Review Board Statement:** Not applicable.

**Informed Consent Statement:** Not applicable.

**Data Availability Statement:** The data presented in this study are available on request from the corresponding author.

**Acknowledgments:** The authors wish to thank I. Hajdara for sample preparation.

**Conflicts of Interest:** The authors declare no conflict of interest.

## References

1. Becker, P. Borate Materials in Nonlinear Optics. *Adv. Mater.* **1998**, *10*, 979–992. [CrossRef]
2. Arun Kumar, R. Borate Crystals for Nonlinear Optical and Laser Applications: A Review. *J. Chem.* **2013**, *2013*, 154862. [CrossRef]
3. Chen, C.; Sasaki, T.; Li, R.; Wu, Y.; Lin, Z.; Mori, Y.; Hu, Z.; Wang, J.; Uda, S.; Yoshimura, M.; et al. *Nonlinear Optical Borate Crystals*; Wiley-VCH GmbH & Co.: Weinheim, Germany; KGaA: Weinheim, Germany, 2012. [CrossRef]
4. Dorenbos, P.; van Eijk, C.W.E. *Proceedings of the International Conference on Inorganic Scintillators and Their Applications, Delft, The Netherlands, 28 August–1 September 1995*; Delft University Press: Delft, The Netherlands, 1996.
5. Knitel, M.J. New Inorganic Scintillators and Storage Phosphors for Detection of Thermal Neutrons. Ph.D. Thesis, Delft University of Technology, Delft, The Netherlands, 1998.
6. Skvortsova, V.; Mironova-Ulmane, N.; Ulmanis, U.; Matkovskii, A. Radiation effects in $Li_2B_4O_7$ oxide crystals. *Nucl. Instrum. Methods Phys. Res. Sect. B Beam Interact. Mater. Atoms* **2000**, *166–167*, 284–288. [CrossRef]
7. Burak, Y.V.; Adamiv, V.T.; Teslyuk, I.M.; Shevel, V.M. Optical absorption of isotopically enriched $Li_2B_4O_7$ single crystals irradiated by thermal neutrons. *Radiat. Meas.* **2004**, *38*, 681–684. [CrossRef]
8. Sangeeta; Chennakesavulu, K.; Desai, D.G.; Sabharwal, S.C.; Alex, M.; Ghodgaonkar, M.D. Neutron flux measurements with a $Li_2B_4O_7$ crystal. *Nucl. Instrum. Methods Phys. Res. Sect. A Accel. Spectrometers Detect. Assoc. Equip.* **2007**, *571*, 699–703. [CrossRef]
9. Singh, A.K.; Tyagi, M.; Singh, S.G.; Tiwari, B.; Desai, D.G.; Sen, S.; Desai, S.S.; Ghodke, S.S.; Gadkaria, S.C. Performance characteristics of thermal neutron detectors based on $Li_6Y(BO_3)_3$:Ce single crystals. *Nucl. Instrum. Methods A* **2015**, *804*, 189–193. [CrossRef]
10. Fawad, U.; Kim, H.J.; Khan, S.; Khan, M.; Ali, L. Photoluminescent properties of white-light-emitting $Li_6Y(BO_3)_3$:$Dy^{3+}$ phosphor. *Solid State Sci.* **2016**, *62*, 1–5. [CrossRef]
11. Singh, A.K.; Singh, S.G.; Tyagi, M.; Desai, D.G.; Sen, S.; Gadkari, S.C. Growth and characterization of lithium yttrium borate single crystals. *AIP Conf. Proc.* **2014**, *1591*, 1250–1252. [CrossRef]
12. Kaewnuam, E.; Wantana, N.; Kim, H.J.; Kaewkhao, J. Development of lithium yttrium borate glass doped with $Dy^{3+}$ for laser medium, W-LEDs and scintillation materials applications. *J. Non-Cryst. Solids* **2017**, *464*, 96–103. [CrossRef]
13. Chaminade, J.P.; Viraphong, O.; Guillen, F.; Fouassier, C.; Czirr, B. Crystal growth and optical properties of new neutron detectors $Ce^{3+}$: $Li_6R(BO_3)_3$ (R = Gd, Y). *IEEE Trans. Nucl. Sci.* **2001**, *48*, 1158–1161. [CrossRef]
14. Tu, C.; Jiang, A.; Luo, Z. The structure of a new laser crystal—$Nd^{3+}$: $Li_6Y(BO_3)_3$ (NLYB). *Jiegou Huaxue Chin. J. Struct. Chem.* **1989**, *8*, 215–219.
15. Yavetski, R.P.; Dolzhenkova, E.F.; Dubovik, M.F.; Korshikova, T.I.; Tolmachev, A.V. Growth of single crystals of $Li_6Y_{1-x}Eu_x(BO_3)_3$ (x = 0–1) solid solutions by the Czochralski method. *Crystallogr. Rep.* **2005**, *50*, 88–91. [CrossRef]
16. Yavetskiy, R.; Tolmachev, A.; Dubovik, M.; Korshikova, T.; Parkhomenko, S. Growth of $Li_6Gd_{1-x}Y_x(BO_3)_3$:$Eu^{3+}$ crystals for thermoluminescent dosimetry. *Opt. Mater.* **2007**, *30*, 119–121. [CrossRef]
17. Yavetskiy, R.; Dolzhenkova, E.; Dubovik, M.; Korshikova, T.; Tolmachev, A. Czochralski growth and optical properties of $Li_6Gd_{1-x}Eu_x(BO_3)_3$ (x = 0–1) single crystals. *J. Cryst. Growth* **2005**, *276*, 485–490. [CrossRef]
18. Lengyel, K.; Tichy-Racs, E.; Timpmann, K.; Vielhauer, S.; Romet, I.; Kovacs, L.; Corradi, G.; Butkus, R.; Vengris, M.; Grigonis, R.; et al. Cooperative luminescence of $Yb^{3+}$ ion pairs in $Li_6Y(BO_3)_3$:Yb single crystals. *J. Lumin.* **2021**, *230*, 117732. [CrossRef]
19. Karunakaran, R.T.; Marimuthu, K.; Babu, S.S.; Arumugam, S. Dysprosium doped alkali fluoroborate glasses-Thermal, structural and optical investigations. *J. Lumin.* **2010**, *130*, 1067–1072. [CrossRef]
20. Kumar, J.S.; Pavani, K.; Babu, A.M.; Giri, N.K.; Rai, S.B.; Moorthy, L.R. Fluorescence characteristics of $Dy^{3+}$ ions in calcium fluoroborate glasses. *J. Lumin.* **2010**, *130*, 1916–1923. [CrossRef]
21. Dominiak-Dzik, G.; Solarz, P.; Ryba-Romanowski, W.; Beregi, E.; Kovács, L. Dysprosium-doped $YAl_3(BO_3)_4$ (YAB) crystals: An investigation of radiative and non-radiative processes. *J. Alloys Compd.* **2003**, *359*, 51–58. [CrossRef]

22. Equall, R.W.; Cone, R.L.; Macfarlane, R.M. Homogeneous broadening and hyperfine structure of optical transitions in $Pr^{3+}$:$Y_2SiO_5$. *Phys. Rev. B* **1995**, *52*, 3963–3969. [CrossRef]
23. Auzel, F. Upconversion and anti-Stokes processes with *f* and *d* ions in solids. *Chem. Rev.* **2004**, *104*, 139–173. [CrossRef]
24. Saha, S.; Kim, H.J.; Khan, A.; Daniel, D.J.; Absar, R.; Barman, R.; Aryal, P.; Kaewkhao, J.; Kothan, S. Luminescence and Scintillation Properties of $Dy^{3+}$ doped $Li_6Y(BO_3)_3$ crystal. *Opt. Mater.* **2020**, *106*, 109973. [CrossRef]
25. Péter, Á.; Polgár, K.; Tóth, M. Synthesis and crystallization of lithium-yttrium orthoborate $Li_6Y(BO_3)_3$ phase. *J. Cryst. Growth* **2012**, *346*, 69–74. [CrossRef]
26. Zhao, Y.W.; Gong, X.H.; Chen, Y.J.; Huang, L.X.; Lin, Y.F.; Zhang, G.; Tan, Q.G.; Luo, Z.D.; Huang, Y.D. Spectroscopic properties of $Er^{3+}$ ions in $Li_6Y(BO_3)_3$ crystal. *Appl. Phys. B* **2007**, *88*, 51–55. [CrossRef]
27. Spassky, D.A.; Kozlova, N.S.; Brik, M.G.; Nagirnyi, V.; Omelkov, S.; Buzanov, O.A.; Buryi, M.; Laguta, V.; Shlegel, V.N.; Ivannikova, N.V. Luminescent, optical and electronic properties of $Na_2Mo_2O_7$ single crystals. *J. Lumin.* **2017**, *192*, 1264–1272. [CrossRef]
28. Dieke, G.H.; Crosswhite, H.M. The Spectra of the Doubly and Triply Ionized Rare Earths. *Appl. Opt.* **1963**, *2*, 675–686. [CrossRef]
29. Macalik, L.; Hanuza, J.; Macalik, B.; Ryba-Romanowski, W.; Golab, S.; Pietraszko, A. Optical spectroscopy of $Dy^{3+}$ ions doped in $KY(WO_4)_2$ crystals. *J. Lumin.* **1998**, *79*, 9–19. [CrossRef]
30. Dominiak-Dzik, G.; Ryba-Romanowski, W.; Lisiecki, R.; Solarz, P.; Berkowski, M. Dy-doped $Lu_2SiO_5$ single crystal: Spectroscopic characteristics and luminescence dynamics. *Appl. Phys. B* **2010**, *99*, 285–297. [CrossRef]
31. Kovács, L.; Casas, S.A.; Corradi, G.; Tichy-Rács, É.; Kocsor, L.; Lengyel, K.; Ryba-Romanowski, W.; Strzep, A.; Scholle, A.; Greulich-Weber, S. Optical and EPR spectroscopy of $Er^{3+}$ in lithium yttrium borate, $Li_6Y(BO_3)_3$:Er single crystals. *Opt. Mater.* **2017**, *72*, 270–275. [CrossRef]
32. Joshi, B.C.; Lohani, R. Non-radiative energy transfer from $Dy^{3+}$ to $Ho^{3+}$ in zinc phosphate glass. *J. Non-Cryst. Solids* **1995**, *189*, 242–245. [CrossRef]
33. Cavalli, E.; Bovero, E.; Belletti, A. Optical spectroscopy of $CaMoO_4$:$Dy^{3+}$ single crystals. *J. Phys. Condens. Matter* **2002**, *14*, 5221–5228. [CrossRef]
34. Rao, B.V.; Buddhudu, S. Emission analysis of $RE^{3+}$ ($Dy^{3+}$ or $Tb^{3+}$):$Ca_3Ln(Y,Gd)(VO_4)_3$ powder phosphors. *Mater. Chem. Phys.* **2008**, *111*, 65–68. [CrossRef]
35. Hsu, C.; Powell, R.C. Energy transfer in europium doped yttrium vanadate crystals. *J. Lumin.* **1975**, *10*, 273–293. [CrossRef]
36. Yu, M.; Lin, J.; Wang, Z.; Fu, J.; Wang, S.; Zhang, H.J.; Han, Y.C. Fabrication, patterning, and optical properties of nanocrystalline $YVO_4$:A (A = $Eu^{3+}$, $Dy^{3+}$, $Sm^{3+}$, $Er^{3+}$) phosphor films via sol-gel soft lithography. *Chem. Mater.* **2002**, *14*, 2224–2231. [CrossRef]
37. Brik, M.G.; Ishii, T.; Tkachuk, A.M.; Tanaka, I. Energy Level Structure of $LiYF_4$:$Dy^{3+}$: Crystal Field Analysis. *Mater. Trans.* **2004**, *45*, 2026–2030. [CrossRef]
38. Carnall, W.T.; Fields, P.R.; Rajnak, K. Electronic Energy Levels in the Trivalent Lanthanide Aquo Ions. I. $Pr^{3+}$, $Nd^{3+}$, $Pm^{3+}$, $Sm^{3+}$, $Dy^{3+}$, $Ho^{3+}$, $Er^{3+}$, and $Tm^{3+}$. *J. Chem. Phys.* **1968**, *49*, 4424–4442. [CrossRef]
39. Kofod, N.; Arppe-Tabbara, R.; Sørensen, T.J. Electronic energy levels of dysprosium(III) ions in solution—Assigning the emitting state, the intraconfigurational 4f-4f transitions in the vis-NIR, and photophysical characterization of Dy(III) in water, methanol and dimethylsulfoxide. *J. Phys. Chem. A* **2019**, *123*, 2734–2744. [CrossRef] [PubMed]